Article

Effects of Electroporation on the Function of Sarco/Endoplasmic Reticulum Ca^{2+}-ATPase and Na^{+},K^{+}-ATPase in H9c2 Cells

Vid Jan, Maida Jusović and Damijan Miklavčič *

Faculty of Electrical Engineering, University of Ljubljana, SI-1000 Ljubljana, Slovenia; vid.jan@fe.uni-lj.si (V.J.); maida.jusovic@gmail.com (M.J.)

* Correspondence: damijan.miklavcic@fe.uni-lj.si

Abstract: Pulsed field ablation (PFA) is a promising new treatment for atrial fibrillation (AF), in which pulmonary vein isolation is achieved by irreversible electroporation. Electroporation causes ATP to leak through the permeabilized membrane. ATP is required both for the healing of the cell membrane and for the functioning of ion pumps, such as sarco/endoplasmic reticulum Ca^{2+}-ATPase (SERCA) or Na^{+},K^{+}-ATPase (NKA), which play a key role in maintaining continuous contractions of the heart muscle. We investigated the effects of electroporation on the expression of ion pumps and possible correlations with the activation of AMPK, the main energy sensor in cells. H9c2 rat cardiac cells were exposed to either monopolar or bipolar (H-FIRE) pulses. Cells lysed 4 or 24 h after electroporation were used for mRNA and protein expression analyses. Overall, both pulse protocols caused a dose-dependent downregulation of crucial SERCA and NKA isoforms, except for NKAα2 and β3, which were upregulated after 24 h. Monopolar pulses also decreased the phosphorylation of FXYD1, which may cause an inhibition of NKA activity. Both pulse protocols caused an increased AMPK activity, which may decrease both SERCA and NKA activity via calcium/calmodulin-dependent protein kinase. Our results provide important new insights into what happens in surviving cardiomyocytes after they are exposed to PFA.

Keywords: irreversible electroporation; reversible electroporation; pulsed field ablation; sarco/endoplasmic reticulum Ca^{2+}-ATPase; Na^{+},K^{+}-ATPase; atrial fibrillation; AMPK activation; H-FIRE pulses; H9c2 cells

1. Introduction

Atrial fibrillation (AF) is the most common arrhythmia encountered in clinical practice, with a prevalence of 0.5% to 2% in the general public [1]. AF can be treated with antiarrhythmic drug therapy, direct cardioversion, and catheter ablation. Catheter ablation with pulmonary vein isolation is considered the most effective treatment of paroxysmal AF (spontaneously terminating AF lasting less than 7 days), persistent AF (lasting more than 7 days), as well as long-standing persistent AF (lasting longer than 1 year) [2].

Pulsed field ablation (PFA), based on irreversible electroporation, is a promising new intervention for the treatment of atrial fibrillation (AF), which isolates electric triggers in pulmonary veins from entering the left atrium and, thus, stops the arrhythmic beating of the heart [3–6]. As PFA is being rapidly introduced into clinical practice, there is growing interest for its use in ventricular tissue as well [7–13]. Electroporation occurs when cells are exposed to short, high-voltage electric pulses [14], which leads to a transient increase in cell membrane permeability and may result in cell death. In PFA, pulses of up to several 1000 Volts and various durations (ns-ms) [15] are delivered via electrodes on a catheter intracardially, causing cell death via non-thermal mechanisms [16]. So far, preclinical and clinical studies showed that PFA represents an effective, efficient, safe, and fast method for the treatment of AF with reduced risk of injuries to the surrounding tissues [17,18]. PFA avoids complications inherent to thermal methods (damage of the esophagus, phrenic nerve paralysis, pulmonary vein stenosis, embolic stroke) [19,20]. Although the main

goal of PFA is irreversible electroporation, it is unavoidable that, in vivo, we also achieve reversible effects [21]. Reversible electroporation occurs (unintentionally) in cells that are located further away from the electrodes/catheter than cells where PFA is performed or (intentionally) during field mapping, as recently suggested [22]. Several unanswered questions remain on how PFA affects cardiac tissue at the cellular level, especially in the areas where reversible electroporation occurs, such as how electroporation affects the contractility of cardiac cells, their pacing, and ion balances, normally regulated by different ion pumps [23–26].

The most important ion pumps for the maintenance of cardiac contractility are sarco/endoplasmic reticulum Ca^{2+}-ATPase (SERCA), plasma membrane Ca^{2+}-ATPase (PMCA), and Na^+,K^+-ATPase (NKA) proteins. SERCA and PMCA pumps work in combination with the sarcolemmal Na^+/Ca^{2+} exchanger and mitochondrial Ca^{2+} uniport to transport Ca^{2+} out of the cytosol (Figure 1A). While SERCA and PMCA only transport 2 Ca^{2+} out of the cytosol, NKA transports 2 K^+ into the cell and, at the same time, transports 3 Na^+ out of the cell. Through this, NKA maintains a negative transmembrane voltage of cardiomyocytes, so they can be subjected to excitation contraction coupling repeatedly. In addition, by maintaining transmembrane voltage, NKA influences cell calcium and contractility by providing the driving force for Ca^{2+} extrusion via the Na^+/Ca^{2+} exchanger.

SERCA, NKA, and PMCA all need ATP to perform their pumping functions. It is reported that 60–70% of generated ATP in the heart is used to fuel contractions, while the remaining 30–40% is mostly used for ion pumps, especially for SERCA [27–29]. Electroporation increases cell plasma membrane permeability, which disrupts the ionic balance (Figure 1B). This creates a demand for ionic pumps to increase their pumping activity to reestablish ionic homeostasis, but, at the same time, ATP is lost through the leaky membrane, which creates an energy shortage in the cells [30–32]. There is barely any literature on how the ion pump function may be affected by electroporation [30,31,33], especially concerning the details of how they are regulated after the cell membrane is so drastically damaged, i.e., electroporated. In most cases, publications correlate tumor cells' higher susceptibility to calcium electroporation compared to normal cells to their downregulation of SERCA and PMCA ion pumps [30,31] but do not explore how electroporation itself may influence the expression levels of ion pumps. We hypothesized that treatment with lower electric fields than lethal may lead to increased expression and activity of ion pumps, while higher electric fields, where the majority of cells do not survive, would cause a downregulation in expression and activity.

One of the pathways that may play a major role in regulating the activity and expression of SERCA, NKA, and PMCA proteins is the 5' AMP-activated protein kinase (AMPK) signaling pathway that regulates catabolic and anabolic processes in cells according to the cell's energy status. AMPK is a heterotrimeric complex that consists of the catalytic α-subunit and the regulatory β- and γ-subunits [34]. It acts as a cellular energy sensor that modulates energy metabolism, cell growth, and cell cycle [35,36] and was recently also implied in membrane repair [37]. When the energy levels are low, AMP binds to the γ-subunit, which, in turn, causes an allosteric activation of AMPK and increases phosphorylation of the α-subunit at Thr172 [38]. AMPK stimulates energy-producing processes and inhibits energy-consuming processes and, thus, restores the energy balance. Interestingly, AMPK has been reported to increase both NKA and SERCA activity in some cases, even though they are both large consumers of energy [39,40], and was activated itself by nanosecond electroporation (nsEP) [41]. Precisely how AMPK activity may relate to SERCA, PMCA, and NKA activity in electroporated cells is unclear.

In our study, we explored how the electroporation of H9c2 rat cardiac myoblast cells using different pulse parameters (i.e., two different waveforms) affects the expression of SERCA and NKA pumps and how electroporation might affect their regulation through the phosphorylation of pumps themselves or their regulatory proteins, phospholamban and phospholemman, respectively. We also evaluated how the electroporation of H9c2 cells affects AMPK activity.
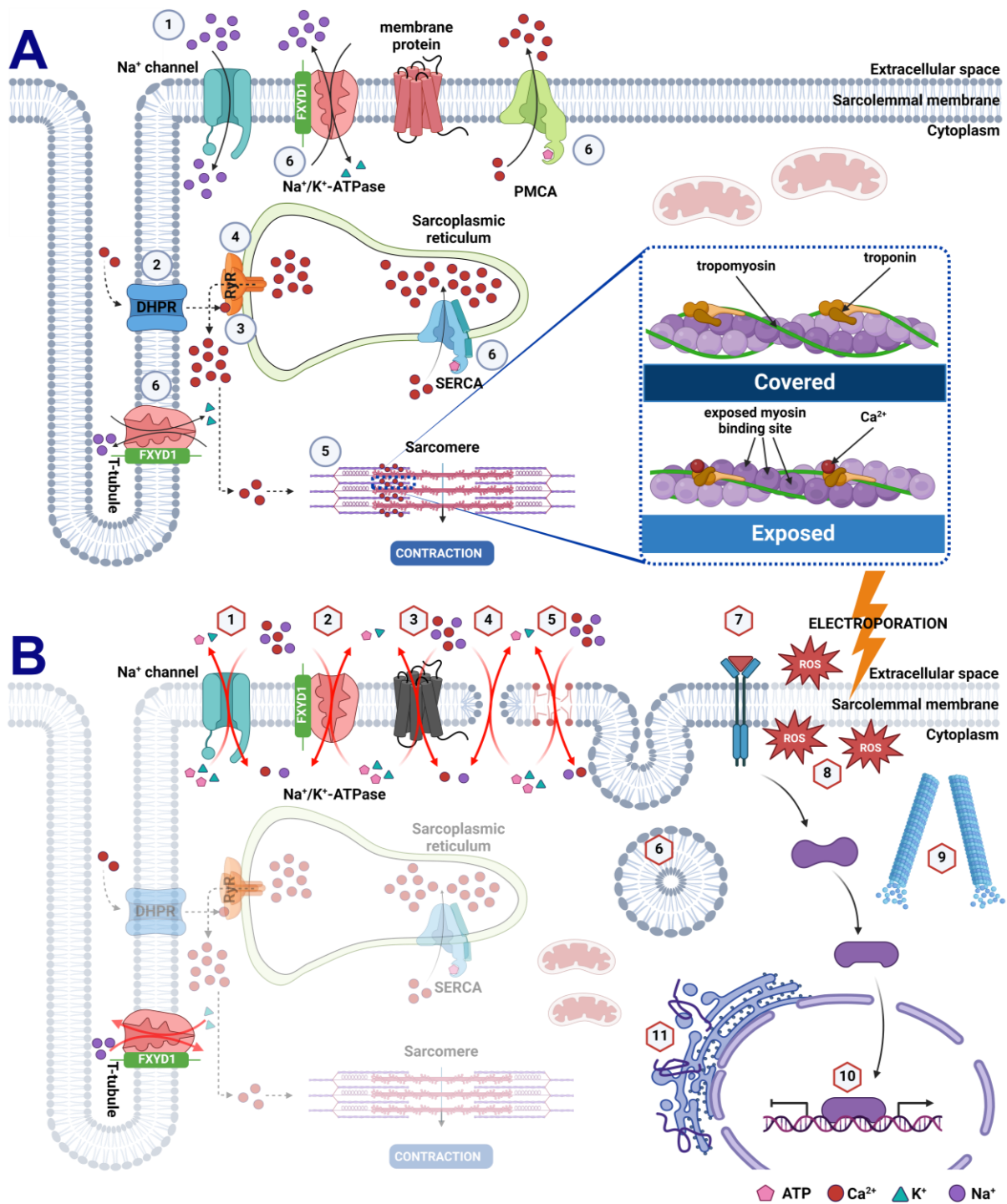
Figure 1. Schemes of excitation contraction coupling in ventricular cardiomyocytes and possible effects of electroporation on cardiomyocyte. (**A**) Action potential spreads along the cell membrane. (1) The rapid depolarization phase is caused by opening of Na$^+$ channels. (2) Depolarization opens L-type Ca^{2+} channels (DHPR) in the T-tubule membrane, which causes small Ca^{2+} uptake into cytosol. (3) Ca^{2+} binds to Ca^{2+} release channels (RyR) in the sarcoplasmic reticulum (SR), which in turn causes (4) release of larger quantities of Ca^{2+}. (5) Released Ca^{2+} binds to the troponin and causes shift of tropomyosin that exposes myosin-binding sites on actin filaments. This enables the contraction. (6) In the relaxation phase some Ca^{2+} is pumped back into SR by SERCA or out of the cell by PMCA, some is transported out of the cell by the Na$^+$/Ca^{2+} exchanger (not shown). Intracellular Na$^+$ homeostasis is achieved by the Na$^+$,K$^+$-ATPase. (**B**) Changes and processes that occur in the cell during and after electroporation.

Electroporation causes activation of (1) ion channels and (2) pumps, (3) protein damage, (4) lipid pore formation, and (5) membrane lipids peroxidation, followed by the release of ATP and K^+ from the cell, influx of Ca^{2+} and Na^+ into the cell, which cause ionic and osmotic imbalance, (6) activation of repair mechanisms and (7) signaling pathways, (8) formation of reactive oxygen species (ROS), (9) cytoskeleton disruption, and changes in (10) gene expression and (11) protein synthesis. Created with Biorender.com.

2. Materials and Methods

2.1. Cells

In this study, H9c2 rat cardiac myoblast cell line (European Collection of Authenticated Cell Cultures ECACC 88092904) was used. The cells were placed and seeded in Dulbecco's Modified Eagle Medium (DMEM, #D6546, Merck, Darmstadt, Germany) supplemented with 4 mM L-glutamine (#G7513, Merck, Germany), 10% FBS (#F2442, Merck, Germany), and a combination of antibiotics, penicillin–streptomycin (#P0781, Merck, Germany) and gentamycin (#G1397, Merck, Germany), with following concentrations: penicillin 1 U/mL, streptomycin 1 µg/mL, and gentamycin 50 µg/mL. Cells were incubated at 37 °C and 10% CO_2.

2.2. Electric Pulse Generation and Electrodes

In this study, two different waveforms (electric pulse parameters) were used to achieve comparable effects with respect to membrane permeabilization and cell survival: monopolar and bipolar high-frequency irreversible electroporation (H-FIRE) pulses. Monopolar treatment of H9c2 cells comprised a total of eight 100 µs pulses (1 Hz repetition frequency), while H-FIRE treatment involved delivery of 100 bursts of 32 bipolar pulses (1 Hz repetition frequency). In addition, H-FIRE signal consisted of pulses with a length of 2 µs, alternating between positive and negative phases, 2 µs pause between the positive and negative phases of each pulse, as well as a 2 µs pause between bipolar pulses. Pulses were delivered using a laboratory prototype pulse generator (University of Ljubljana, Ljubljana, Slovenia), which is based on H-bridge digital amplifier with 1 kV MOSFETs (DE275-102N06A, IXYS, Milpitas, CA, USA) [42]. A high-voltage differential probe HVD3206A (Teledyne LeCroy, Chestnut Ridge, NY, USA), current probe, CP031 (Teledyne LeCroy, Chestnut Ridge, NY, USA), and oscilloscope WaveSurfer 3024z 200 MHz (Teledyne LeCroy, Chestnut Ridge, NY, USA) were used to measure the delivered pulses [43–45]. Cells were subjected to electric pulses by being positioned between two parallel stainless-steel electrodes. Electric field was determined by dividing the voltage applied with the distance between the electrodes (2 mm).

2.3. Determining Plasma Membrane Permeability and Resealing

For permeability tests, 60 µL of cell suspension was combined with 6 µL of 1.5 mM propidium iodide (PI, final concentration of 136 µM) shortly before the pulses were delivered. Then, 60 µL of cell suspension was electroporated, after which 50 µL of the treated sample was moved to a 1.5 mL centrifuge tube. Three minutes after electroporation (permeability experiments), the samples were diluted in 150 µL of DMEM and mixed using a vortex. The uptake of PI was assessed using the flow cytometer (Attune NxT; Life Technologies, Carlsbad, CA, USA). Cells were excited with a blue laser at 488 nm, and the emitted fluorescence was measured using a 574/26 nm band-pass filter. The measurement reached 10,000 acquired events. Gating was used to separate individual cells from debris and clusters using dot-plots for forward and side scatter, with reference to the sham control (0 V/cm). The Attune NxT program was used to analyze the obtained data. A histogram of PI fluorescence was used to calculate the percentage of permeabilized cells [46].

2.4. Determining Cell Survival Following Electroporation

For this, 60 µL of cell suspension was electroporated, after which 50 µL of the treated sample was moved to a 1.5 mL centrifuge tube. Three minutes after electroporation, the cells were thoroughly mixed with a pipette and diluted in 350 µL of DMEM. After

the exposure to the treatment protocol, each sample was transferred in three technical repetitions (2×10^4 cells per well, V = 100 μL) on a 96-well plate (TPP, Trasadingen, Switzerland). Following a 24 h incubation at 37 °C and humidified 5% CO_2, a survival assay was conducted. Then, 20 μL of MTS tetrazolium compound (CellTiter 96® AQueous One Solution Cell Proliferation Assay (MTS), Promega, Madison, WI, USA) was added to each well according to manufacturer's instructions and incubated for 2 h. The number of viable cells was determined using MTS assay by evaluating the metabolic activity of cells and by measuring the formazan absorbance at 490 nm. Following a 2 h incubation period, the absorbance was measured by a spectrofluorometer (Tecan Infinite 200; Tecan, Grödig, Austria). To calculate cell survival, the background (containing only DMEM and MTS) was subtracted from all measurements, and then the absorbance of the treated samples was normalized to that of the control samples.

2.5. Cell Treatments for qPCR and Immunoblotting Analyses

We tested for voltage between 0 and 250 V with increments of 50 V, resulting in electric field between 0 and 1250 V/cm, estimated by voltage divided by distance between the stainless-steel plate electrodes. The cell density used throughout experiments was 1.5×10^7 cells/mL. After electroporation, 60 μL of the treated cells was diluted to appropriate concentration in culture medium, placed in 6-well plates, and incubated for 4 and 24 h (2 mL of cell suspension per well). Further, 2.25×10^5 cells were seeded per well for 4 h incubation, while 1.5×10^5 cells were seeded per well for 24 h incubation. Incubation times were chosen based on our previous research [46]. The culture medium was then removed, and the cells were rinsed twice with ice-cold PBS and stored at −80 °C for further analysis, which involved quantitative PCR and/or immunoblotting.

2.6. Quantitative Real-Time PCR (qPCR)

The total RNA was extracted from H9c2 cells with E.Z.N.A Total RNA kit I (Omega, Bio-Tek, Norcross, GA, USA, cat. no. R6834). Reverse transcription was performed using High-Capacity cDNA Reverse Transcription Kit (Thermo Fisher Scientific, Waltham, MA, USA, cat. no. 4368814). TaqMan Universal Master Mix used in this experiment was from Thermo Fisher Scientific (cat. no. 4364340). Both reverse-transcription and quantitative real-time PCR (qPCR) were performed using QuantStudio 3 (Thermo Fisher Scientific, Waltham, MA, USA). qPCR analysis was performed using TaqMan Gene Expression Assays (Thermo Fisher Scientific, Waltham, MA, USA): NKA alfa 1 (*Atp1a1*, cat. no. 4448892, Rn01533986_m1), NKA alfa 2 (*Atp1a2*, cat. no. 4448892, Rn00560789_m1), NKA alfa 3 (*Atp1a3*, cat. no. 4448892, Rn00560813_m1), NKA beta 1 (*Atp1b1*, cat. no. 4448892, Rn00565405_m1), NKA beta 2 (*Atp1b2*, cat. no. 4448892, Rn00560819_m1), NKA beta 3 (*Atp1b3*, cat. no. 4448892, Rn00755009_m1), Phospholemman (*Fxyd1*, cat. no. 4448892, Rn00581299_m1), phospholamban (*Pln*, (cat. no. 4453320, Rn01434045_m1), SERCA1 (*Atp2a1*, cat. no. 4448892 Rn01508014_m1), SERCA2 (*Atp2a2*, cat. no. 4453320, Rn00568762_m1), SERCA3 (*Atp2a3*, cat. no. 4448892, Rn00563800_m1), 18S (cat. no. 4331182, Hs99999901_s1), and Cyclophilin A (*Ppia*, cat. no. 4331182, Rn00690933_m1). Results are reported as gene expression ratios (Equation (1)):

$$\left(1 + E_{reference}\right)^{Ct,\ reference} / \left(1 + E_{target}\right)^{Ct,\ target} \tag{1}$$

where *E* represents PCR efficiency, while *Ct* represents threshold cycle [47,48]. Gene expression levels of evaluated proteins were normalized to geometric mean of endogenous controls 18S rRNA and Ppia [48]. Figure 2 shows the mRNA expression levels of distinct NKA and SERCA isoforms, as well as their respective regulators, FXYD1 and phospholamban.
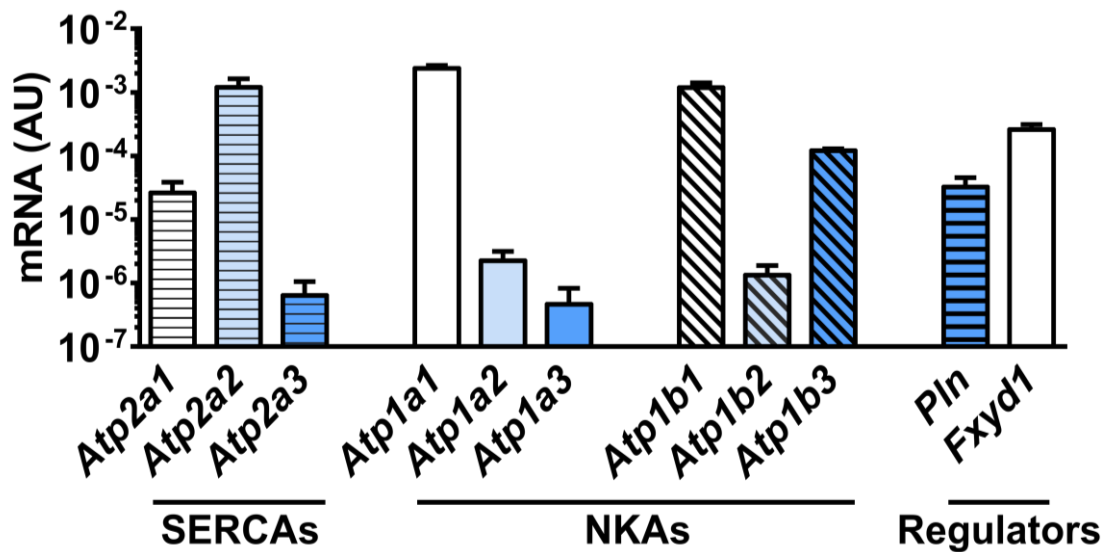
Figure 2. Comparison of mRNA expression levels of different sarco/endoplasmic reticulum Ca^{2+}-ATPase (SERCA) isoforms, Na^+,K^+-ATPase (NKA) subunits, and their regulators phospholamban (Pln) and phospholemman (FXYD1), respectively, in H9c2 cells. qPCR was used to evaluate basal levels of gene expression for SERCA1-3 (*Atp2a1-3*), NKAα1-3 (*Atp1a1-3*), NKAβ1-3 (*Atp1b1-3*), and their regulators phospholamban (*Pln*), and phospholemman (*Fxyd1*), respectively. qPCR was performed using rat-specific gene expression assays, normalized to geometric mean of 18S and PPIA endogenous controls. Results are means ± SD (n = 7).

2.7. Immunoblotting

Electroporated H9c2 cells were cultured in 6-well plates in complete medium and left to attach for 4 and 24 h in incubator. Next, cells were lysed with Pierce™ RIPA buffer (#89901, Thermo Fisher Scientific, Waltham, MA, USA), and their protein concentration was determined using the Pierce BCA Protein Assay Kit (#23225 and 23227, Thermo Fisher Scientific, Waltham, MA, USA), following the manufacturer's guidelines. Each sample within every replication was adjusted to the identical concentration prior to separation. The proteins were separated using Bolt™ 4–12%, Bis-Tris, 1.0 mm, Mini Protein Gels (#NW04125BOX, Thermo Fisher Scientific, Waltham, MA, USA), and Mini Gel Tank (#A25977, Thermo Fisher Scientific, Waltham, MA, USA) and then transferred onto PVDF membranes using Power Blotter Select Transfer Stacks (mini, #PB5210, Thermo Fisher Scientific, Waltham, MA, USA) and Power Blotter-Semi-dry Transfer System (Thermo Fisher Scientific, Waltham, MA, USA), following the manufacturer's guidelines. Ponceau S (0.1% (*w/v*) in 5% (*v/v*) acetic acid) staining was used to assess loading and transfer efficiency. After transfer, membranes were blocked with 7.5% (*w/v*) dry skimmed milk in Tris-buffered saline with Tween (TBST: 20 mM Tris, 150 mM NaCl, 0.02% (*v/v*) Tween 20, pH 7.5) for 1 h at room temperature. Following this, the membranes were incubated overnight at 4 °C with different primary antibodies in a solution containing 20 mM Tris, 150 mM NaCl, pH 7.5, 0.1% (*w/v*) BSA, and 0.1% (*w/v*) NaN₃. Additional information regarding primary antibodies used in this study can be found in Table 1.

Following several washing steps in TBST solution, membranes were incubated with a secondary antibody horseradish peroxidase conjugate in TBST with 5% (*w/v*) dry skimmed milk for 1 h at room temperature. After additional washing steps in TBST, membranes were incubated with Pierce Enhanced Chemiluminescence reagent (#32106, Thermo Fisher Scientific, Waltham, MA, USA) for 1 min, after which bands were visualized and quantified using Uvitec Alliance Q9 (Uvitec, Cambridge, UK) and Quantity One 1-D Analysis Software 4.6.8. (Bio-Rad, Hercules, CA, USA).

Table 1. List of primary antibodies used in this study.

Antibody	Host	Type	Dilution	Supplier	Cat. No.
NKAα1 Tyr10	Rabbit	Monoclonal	1:500	CST	13566
NKAβ1	Rabbit	Monoclonal	1:1000	CST	62849
NKAβ2	Rabbit	Polyclonal	1:500	TFS	PA5-121248
NKAβ3 (CD298)	Rabbit	Monoclonal	1:1000	Invitrogen	MA5-37934
SERCA1	Rabbit	Polyclonal	1:1000	CST	4219
SERCA2	Rabbit	Monoclonal	1:1000	CST	9580
Pln	Rabbit	Monoclonal	1:500	CST	14562
Pln Ser16/Thr17	Rabbit	Polyclonal	1:1000	CST	8496
ACC	Rabbit	Monoclonal	1:1000	CST	3676
AMPKα	Rabbit	Polyclonal	1:1000	CST	2532
pAMPKα Thr172	Rabbit	Monoclonal	1:1000	CST	2535
pACC Ser79	Rabbit	Polyclonal	1:1000	CST	3661
NKAα1	Mouse	Monoclonal	1:2000	Merck	05-369
NKAα2	Rabbit	Polyclonal	1:4000	Merck	AB9094-I
NKAα3	Mouse	Monoclonal	1:1000	TFS	MA3-915
FXYD1	Rabbit	Polyclonal	1:1000	Invitrogen	PA5-79288
pFXYD1 Ser68	Rabbit	Polyclonal	1:500–2000	TFS	PA5-99971

CST: Cell Signaling Technology; TFS: Thermo Fisher Scientific.

2.8. Statistical Analyses

The data are presented as means ± SD. All statistical analyses were performed using GraphPad Prism 6 (version 6.01, GraphPad Software, Boston, MA, USA). Statistical significance ($p < 0.05$) was determined by a two-way ANOVA followed by Dunnett's post hoc test for assessing multiple comparisons. 'n' represents the number of biological replicates included in the analysis.

3. Results

In our study, we investigated how the electroporation (irreversible and reversible) of H9c2 cells achieved by different pulse parameters affects the expression of SERCA and NKA pumps and how electroporation might affect their regulation through the phosphorylation of pumps themselves or through phosphorylation of their regulatory proteins, phospholamban and pholemman, respectively. We also investigated how the electroporation of H9c2 cells affects AMPK activity.

3.1. Plasma Membrane Permeability and Survival of H9c2 Cells after Electroporation

We first determined the range of pulse amplitudes causing membrane electroporation—reversible and irreversible (i.e., cell death)—which we later used in experiments for gene and protein expression. We selected a range of treatment intensities, from electric fields where no electroporation was observed (low percentage of membrane permeabilization and high survival) to high electric fields where most cells were irreversibly electroporated, as determined by permeabilization and cell survival assays, but, still, enough cells survived for protein and RNA extraction. In Figure 3, we can see that at 1250 V/cm, we achieved a high percentage of permeabilized cells and cell survival of less than 20% with both monopolar and H-FIRE pulses. As H-FIRE pulses are less effective than monopolar pulses at the same exposure times, we used longer cumulative exposure times for H-FIRE pulses (100 bursts of 32 pulses of 2–2–2–2 μs, 12,800 μs) than monopolar pulses (800 μs). We, thus, selected 0, 300, 500, 750, 1000, and 1250 V/cm to treat H9c2 cells for the gene and protein evaluation.

3.2. Effect of Electroporation on SERCA mRNA and Protein Expression

The electroporation of cells can have several negative effects on homeostasis (Figure 1B). The disruption of ion balance and ATP loss due to electroporation have severe effects on the normal function of ion pumps. It was reported that low expression levels of SERCAs and

PMCAs may play a role in the higher sensitivity of tumor cells compared to normal cells to calcium electroporation [30,31,49]. Thus, we investigated how electroporation may affect the expression of SERCA isoforms 1, 2, and 3 and the expression and phosphorylation of the SERCA regulator phospholamban (Pln).
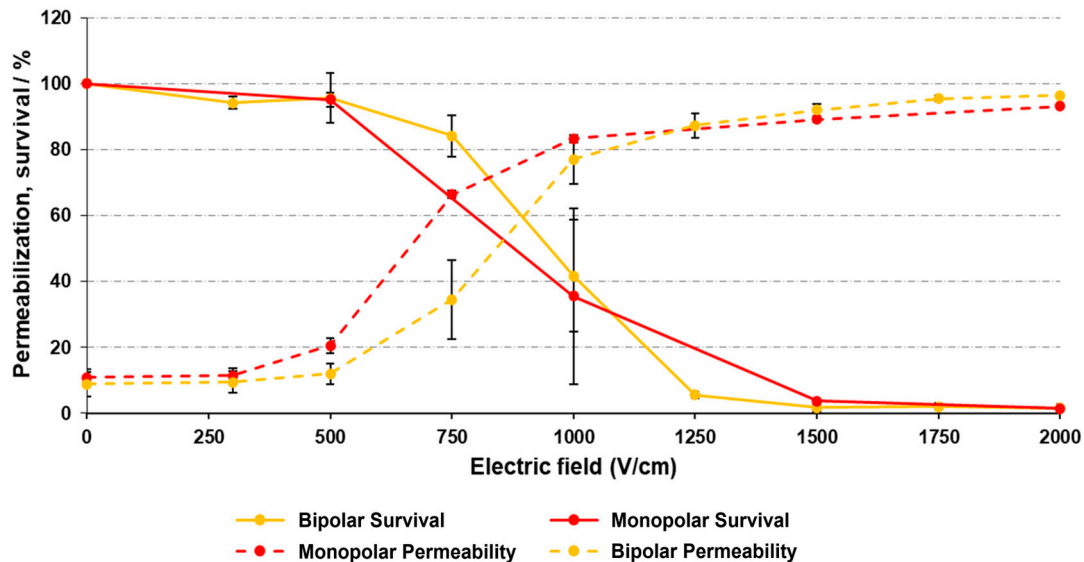

Figure 3. Evaluation of plasma membrane permeability and survival of H9c2 cells after electroporation. Cells were treated with either 8 × 100 μs long monopolar pulses (Monopolar; 1 Hz repetition frequency), or 100 bursts of 32 short bipolar pulses (H-FIRE) of 2–2–2–2 μs (bipolar; 1 Hz repetition frequency, pulses of 2 μs duration of positive and negative phase, 2 μs pause between positive and negative phase, 2 μs pause between bipolar pulses). The uptake of PI, measured by the flow cytometer 3 min after electroporation, was used to evaluate permeability of plasma membrane, while MTS viability assay was used to evaluate cell survival 24 h after electroporation. Results are means ± SD (n = 3–4).

Regarding mRNA levels, a significant decrease in the expression of SERCA1 (*Atp2a1*) was observed within the first 24 h following electroporation, with both monopolar and H-FIRE pulses (Figure 4A,D). The same was also observed at the protein level, where both monopolar and H-FIRE pulses caused a downregulation in expression at 4 and 24 h (Figure 4G,J). On the contrary, the mRNA expression of SERCA2 (*Atp2a2*) remained stable, as can be seen in Figure 4B,E, but we detected a downregulation in the protein level, which was significant at 4 h for H-FIRE pulses but not for monopolar pulses (Figure 4H,K). SERCA3 mRNA levels were very low (Figure 2), but we nevertheless detected an increase in the expression 4 h after electroporation with both monopolar and H-FIRE pulses (Figure 4C,F). We also evaluated the mRNA expression of phospholamban (*Pln*) but were unsuccessful in detecting it at the protein level. At the mRNA level, phospholamban levels were significantly increased at the basal level when comparing 4 to 24 h (Figure 4I,L), but 24 h after electroporation with higher electric fields, the expression was reduced to the 4 h basal levels.

3.3. Effects of Electroporation on the Expression of NKA α-Subunits

As ion imbalance and a loss of ATP also affect the function of NKA (Figure 1B), we were interested in how electroporation with monopolar or H-FIRE pulses affects its expression and function. We first evaluated the expression of catalytic α-subunits (1–3) at the mRNA and protein levels.
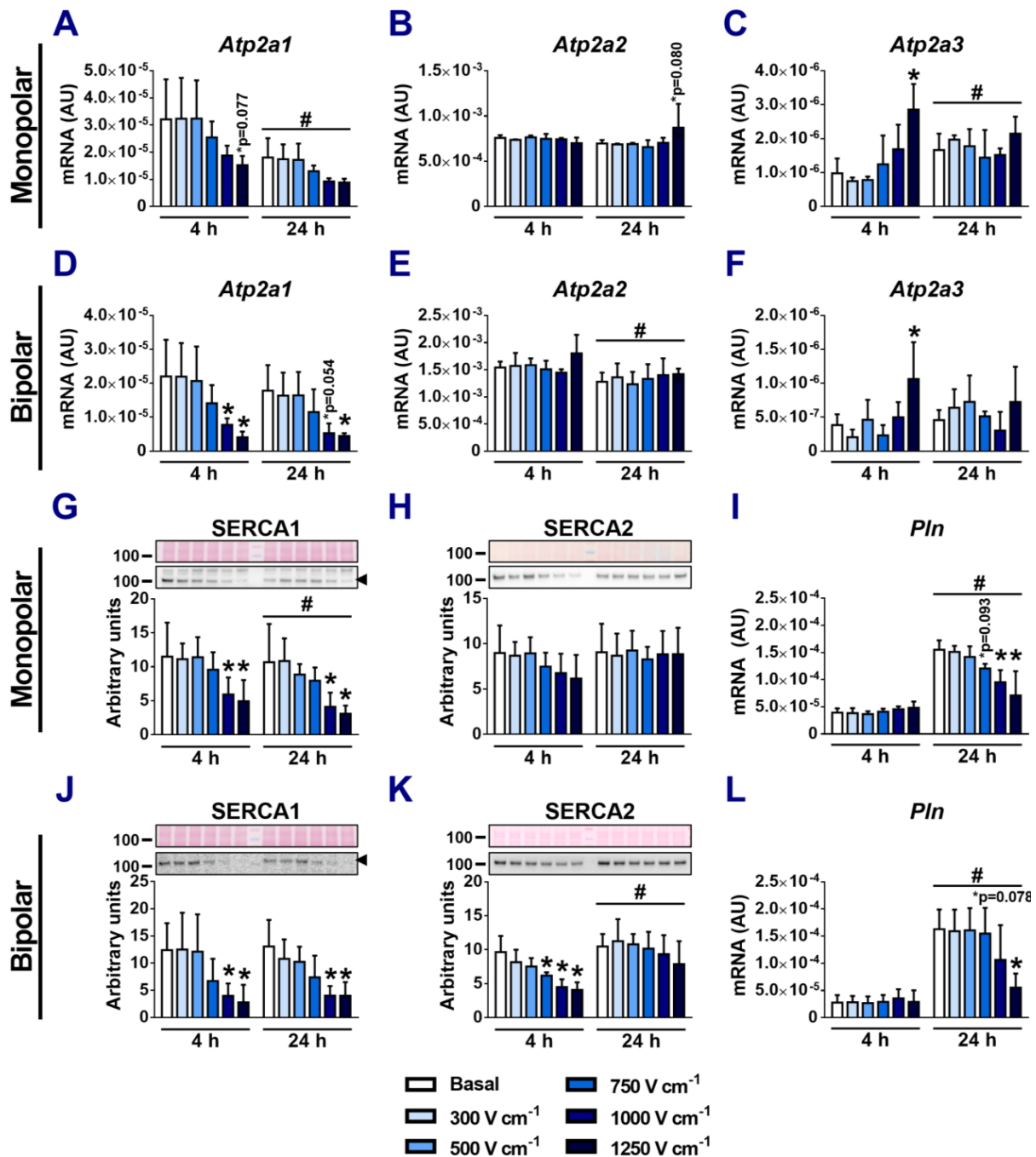
Figure 4. Effects of different types of electric pulses (monopolar and bipolar) on mRNA and protein expression of SERCA isoforms and phospholamban (Pln) in H9c2 cells. (**A–F**) qPCR was used to determine gene expression of SERCA1-3 (*Atp2a1-3*) subunits following electroporation for indicated time periods. (**G,H,J,K**) Immunoblotting was used to estimate protein abundance of SERCA1 and 2 isoforms following electroporation for indicated time periods. Total protein loading was evaluated by Ponceau S staining (shown above the blots). Numbers next to the blots and Ponceau stains indicate molecular weight markers in kDa. Black arrowheads indicate the analyzed bands when unspecific bands were detected, (**I,L**) qPCR was used to determine gene expression of phospholamban (*Pln*) following electroporation for indicated time periods. qPCR was performed using rat-specific gene expression assays, normalized to geometric mean of 18S and PPIA endogenous controls. Values on the graphs are means $\pm$ SD (n = 3–4 for qPCR, n = 6–8 for immunoblotting) and results that are statistically significant are indicated (* $p < 0.05$ vs. Basal; # $p < 0.05$ 4 h vs. 24 h. Two-way ANOVA with Dunnet's post hoc adjustment was used for statistical evaluation).

At the mRNA level, we observed no effects of electroporation on the expression of NKAα1 (*Atp1a1*) with both monopolar and H-FIRE pulses (Figure 5A,D). After electroporation with monopolar pulses, we observed a non-significant trend in the downregulation of NKAα2 (*Atp1a2*) at the mRNA level, after both 4 and 24 h (Figure 5B), as a function of treatment intensity. H-FIRE pulses caused a significant downregulation after 24 h (Figure 5E). We also observed an upregulation in the mRNA expression of NKAα3 (*Atp1a3*), 24 h after being treated with H-FIRE pulses at 1250 V/cm (Figure 5F). It is important to note, however, that the expression levels of NKA α3 were the lowest of the 3 alpha subunits, so the relevance of this result might be negligible (Figure 2).

At the protein level, we observed a downregulation in the expression of NKAα1 for monopolar pulses after 24 h at 1250 V/cm (Figure 5G), while H-FIRE pulses caused a downregulation after 4 h and at electric field values from 500 to 1250 V/cm (Figure 5J). H-FIRE pulses caused a significant downregulation in the protein expression of NKAα2 after 4 h, while both monopolar and H-FIRE pulses increased the expression at high electric fields after 24 h (Figure 5H,K). We also detected a downregulation in the expression of NKAα3 after 4 h in cells treated with monopolar pulses (Figure 5I), but as at the mRNA level, due to the low overall expression levels of the α3 subunit in H9c2 cells, these results may not have an important effect on the function of treated cells. Overall, the trends of the effects of electroporation on the expression of NKA α-subunits seem to be similar between both monopolar and bipolar H-FIRE pulses.

3.4. Effects of Electroporation on the Expression of NKA β-Subunits

We also analyzed the effects of electroporation with monopolar and H-FIRE pulses on the expression of NKA β-subunits, which are crucial for the assembly, maturation, and function of α/β-heterodimers.

We observed a significant upregulation in the mRNA expression of NKAβ1 (*Atp1b1*) with both monopolar and H-FIRE pulses after 4 h, while this upregulation was less evident after 24 h (Figure 6A,D). We observed no effects of electroporation on the protein expression of NKAβ1, neither with monopolar nor H-FIRE pulses (Figure 6G,J). NKAβ2 subunit (*Atp1b2*) expression was by far the lowest of the three NKA β-subunits (Figure 2). We observed no changes at the mRNA level with either electroporation protocol (Figure 6B,E). We did, however, detect an upregulation in the protein expression of NKAβ2 24 h after cells were treated with monopolar pulses (Figure 6H), but like with the NKAα3 results before, these changes most probably do not have significant consequences for the functioning of the cells due to the low expression levels of NKA β2. NKAβ3 (*Atp1b3*) mRNA levels were increased 24 h after cells were treated with monopolar pulses at 1250 V/cm (Figure 6C). At the protein level, both monopolar and H-FIRE pulses caused a downregulation in the expression of NKAβ3, but this effect seems to have diminished after 24 h and actually turned into an upregulation in cells treated with bipolar pulses (Figure 6I,L).

3.5. Effects of Electroporation on Phosphorylation of NKAα1 and FXYD1

To gain a deeper understanding of how electroporation with different pulse parameters affects NKA ion pump activity, we also examined the phosphorylation status of NKAα1 (Tyr10) and phosphorylation and the expression of the NKA regulator FXYD1 (Figure 7).

There was a slight but non-significant decrease in the phosphorylation of the NKAα1 subunit on the Tyr10 residue 24 h after exposure to both types of pulses (Figure 7A,D). Monopolar pulses had no effect on phosphorylation of NKAα1 subunit 4 h after treatment (Figure 7A), while H-FIRE pulses increased phosphorylation 4 h after treatment at 1000 and 1250 V/cm (Figure 7D). This effect was also observed when we normalized the phosphorylated protein to total (Figure 7E).
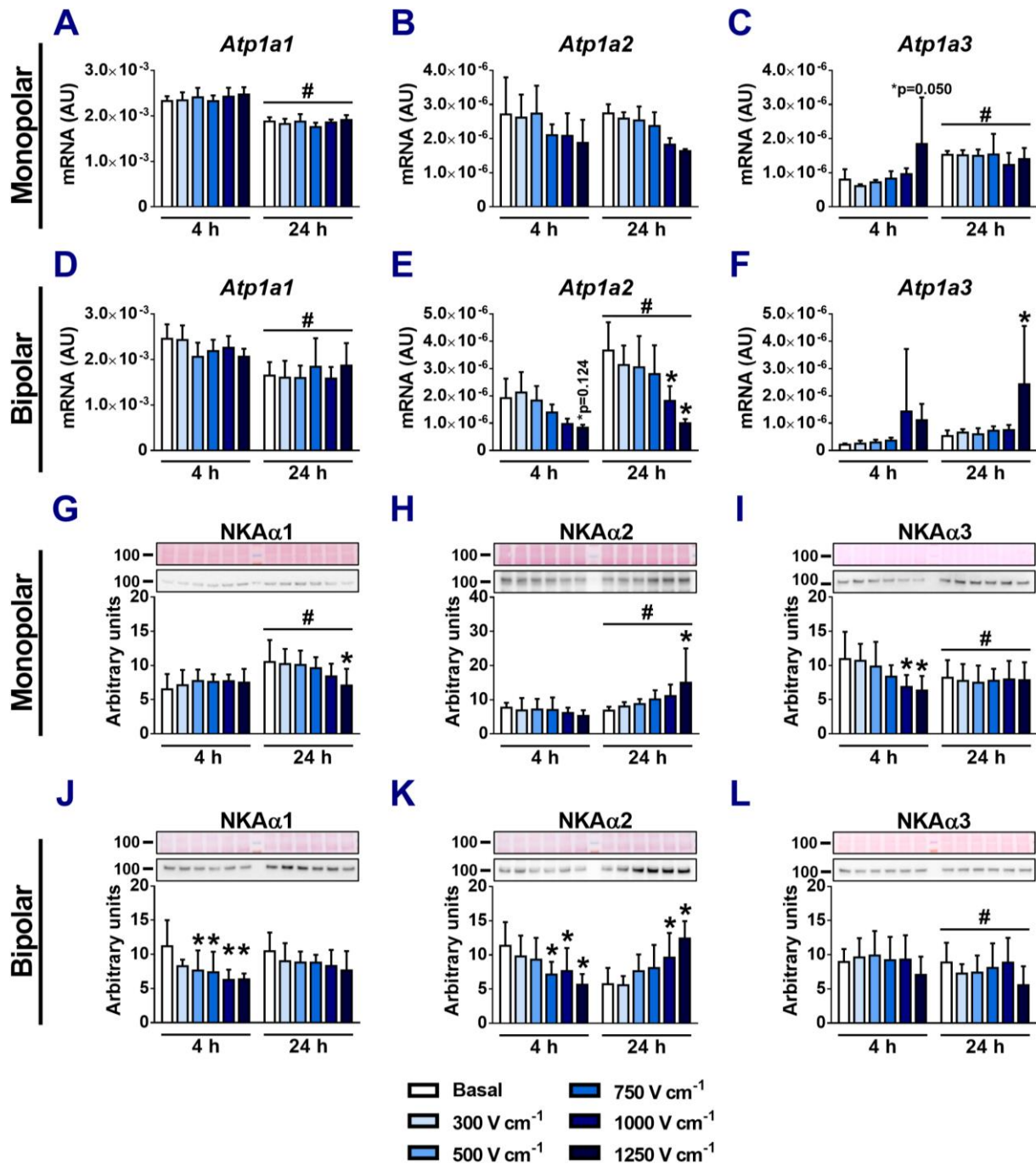
Figure 5. Effects of different types of electric pulses (monopolar and bipolar) on mRNA and protein expression of NKA α subunits in H9c2 cells. (**A–F**) qPCR was used to determine gene expression of NKAα1-3 (*Atp1a1-3*) subunits following electroporation for indicated time periods. (**G–L**) Immunoblotting was used to estimate protein abundance of NKA α1-3 following electroporation for indicated time periods. Total protein loading was evaluated by Ponceau S staining (shown above the blots). Numbers next to the blots and Ponceau stains indicate molecular weight markers in kDa. qPCR was performed using rat-specific gene expression assays, normalized to geometric mean of 18S and PPIA endogenous controls. Values on the graphs are means ± SD (n = 3–4 for qPCR, n = 7–8 for immunoblotting) and results that are statistically significant are indicated (* $p < 0.05$ vs. basal; # $p < 0.05$ 4 h vs. 24 h). Two-way ANOVA with Dunnet's post hoc adjustment was used for statistical evaluation).
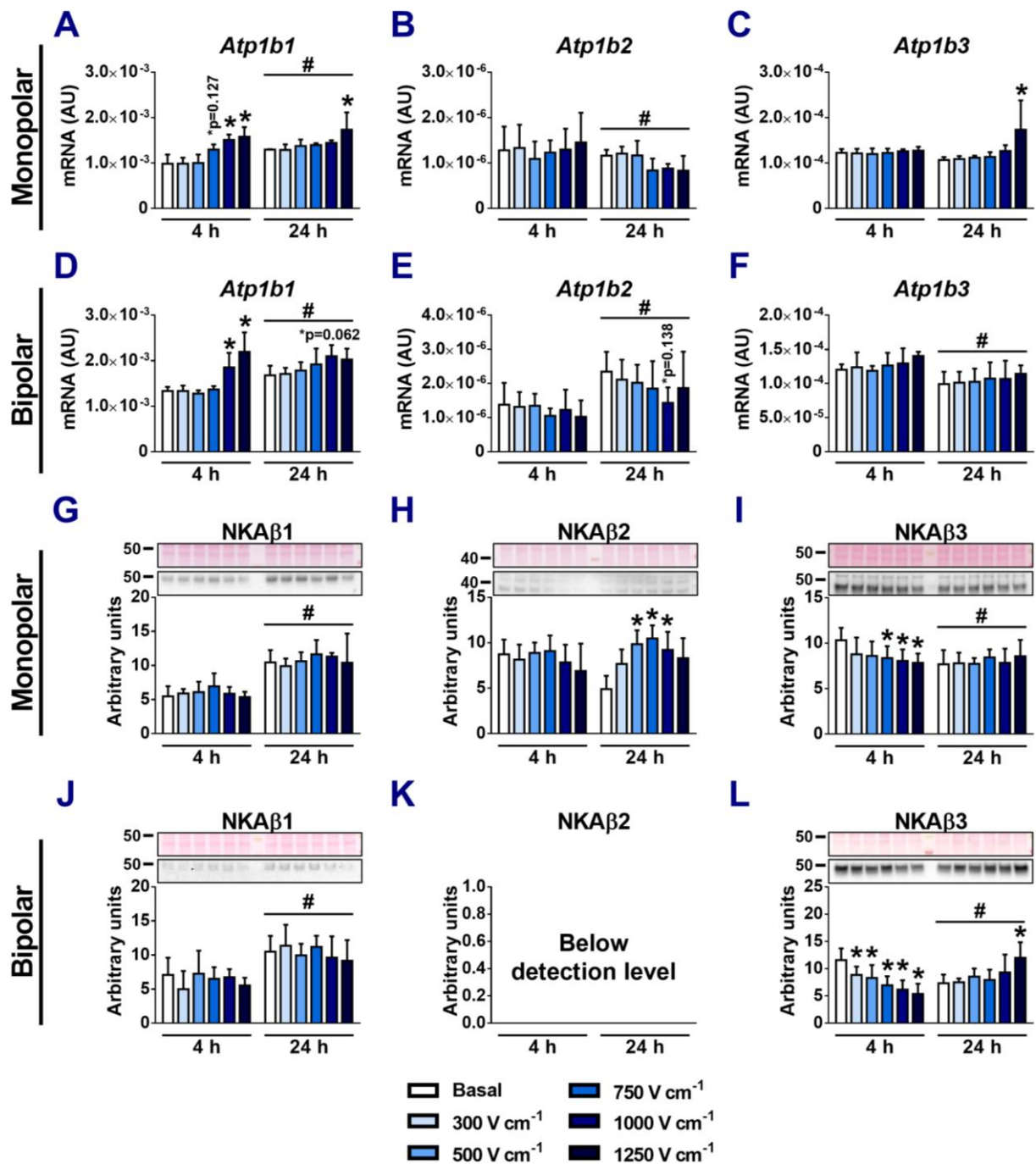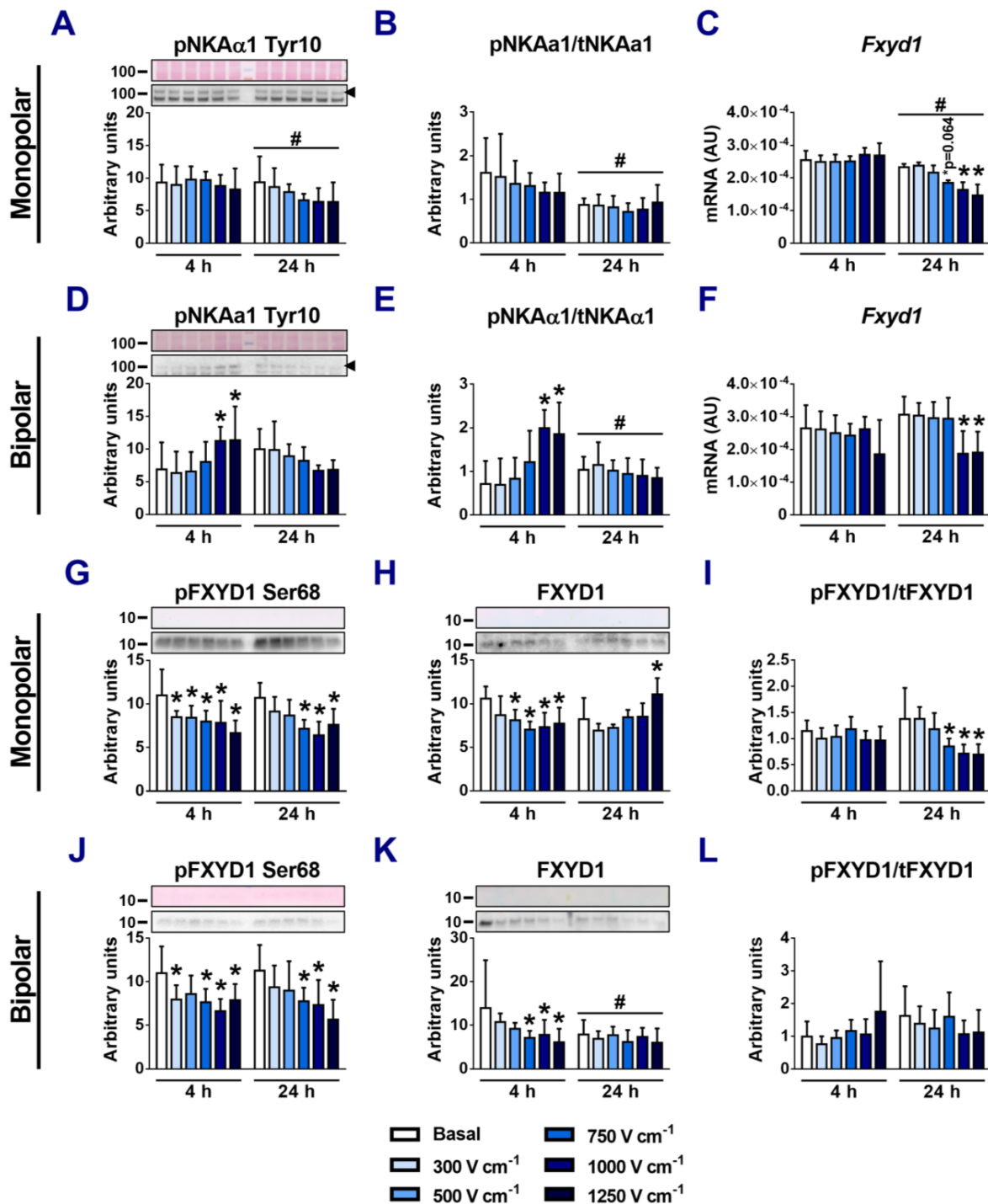
Figure 6. Effects of different types of electric pulses (monopolar and bipolar) on mRNA and protein expression of NKA β subunits in H9c2 cells. (**A–F**) qPCR was used to determine gene expression of NKAβ1-3 (*Atp1b1-3*) subunits following electroporation for indicated time periods. (**G–L**) Immunoblotting was used to estimate protein abundance of NKAβ1-3 following electroporation for indicated time periods. Total protein loading was evaluated by Ponceau S staining (shown above the blots). Numbers next to the blots and Ponceau stains indicate molecular weight markers in kDa. qPCR was performed using rat-specific gene expression assays, normalized to geometric mean of 18S and PPIA endogenous controls. Values on the graphs are means ± SD (n = 3–4 for qPCR, n = 3–8 for immunoblotting) and results that are statistically significant are indicated (* $p < 0.05$ vs. basal; # $p < 0.05$ 4 h vs. 24 h). Two-way ANOVA with Dunnet's post hoc adjustment was used for statistical evaluation).

Figure 7. Effects of different types of electric pulses (monopolar and bipolar) on phosphorylation of NKAα1 and FXYD1. (**A**,**B**,**D**,**E**,**G**–**L**) Immunoblotting was used to estimate pNKAα1 Tyr10, phosphorylation of NKAα1 relative to total protein, pFXYD1 Ser68, FXYD1, and phosphorylation of FXYD1 relative to total protein. Total protein loading was evaluated by Ponceau S staining (shown above the blots). Numbers next to the blots and Ponceau stains indicate molecular weight markers in kDa. Black arrowheads indicate the analyzed bands when unspecific bands were detected. (**C**,**F**) qPCR was used to determine gene expression of FXYD1. qPCR was performed using rat-specific gene expression assays, normalized to geometric mean of 18S and PPIA endogenous controls. Values on the graphs are means $\pm$ SD (n = 3–4 for qPCR, n = 6–8 for immunoblotting) and results that are statistically significant are indicated (* $p < 0.05$ vs. Basal; # $p < 0.05$ 4 h vs. 24 h). Two-way ANOVA with Dunnet's post hoc adjustment was used for statistical evaluation).

In addition to the phosphorylation of NKAα1 itself, we also investigated how electroporation affects the expression and phosphorylation of FXYD1. FXYD1 is the main regulator of NKA in cardiac cells. The unphosphorylated form of FXYD1 inhibits the activity of NKA, while the phosphorylated form increases it. We observed a downregulation in the mRNA expression of FXYD1 after 24 h with both monopolar and H-FIRE pulses (Figure 7C,F). At the protein level, we observed a downregulation in both the phosphorylation and total protein content after 4 h with monopolar and H-FIRE pulses (Figure 7G,H,J,K), although we did see an upregulation in the total protein content with monopolar pulses at 24 h at 1250 V/cm (Figure 7H). When phosphorylated FXYD1 was normalized to total FXYD1, we observed a significant downregulation in the ratio of the phosphorylated form with monopolar pulses and a negative trend with H-FIRE pulses at 24 h, which may suggest that NKA activity is inhibited by FXYD1, 24 h after H9c2 cells are exposed to electric fields, causing the highest cell electroporation/membrane permeability (Figure 7I,L).

3.6. The Role of AMPK in Regulation of NKA Ion Pump Activity in Electroporated Cells

AMP-activated protein kinase (AMPK) is an enzyme that plays a vital role in regulating cellular energy homeostasis in response to various metabolic stresses. Typically, AMPK is activated in response to energy stress. The activation of AMPK can stimulate or inhibit the activity of NKA, and it is also known that AMPK can affect SERCA activity. AMPK is regulated at multiple levels, including post-translational modifications. One of the most important post-translational modifications that activate AMPK is the phosphorylation of a specific threonine residue (Thr172) within the activation loop of the kinase domain. We, thus, investigated how the electroporation of H9c2 cells with either monopolar or bipolar H-FIRE pulses might affect the activity of AMPK and of its direct target, Acetyl-CoA carboxylase (ACC) (Figure 8).
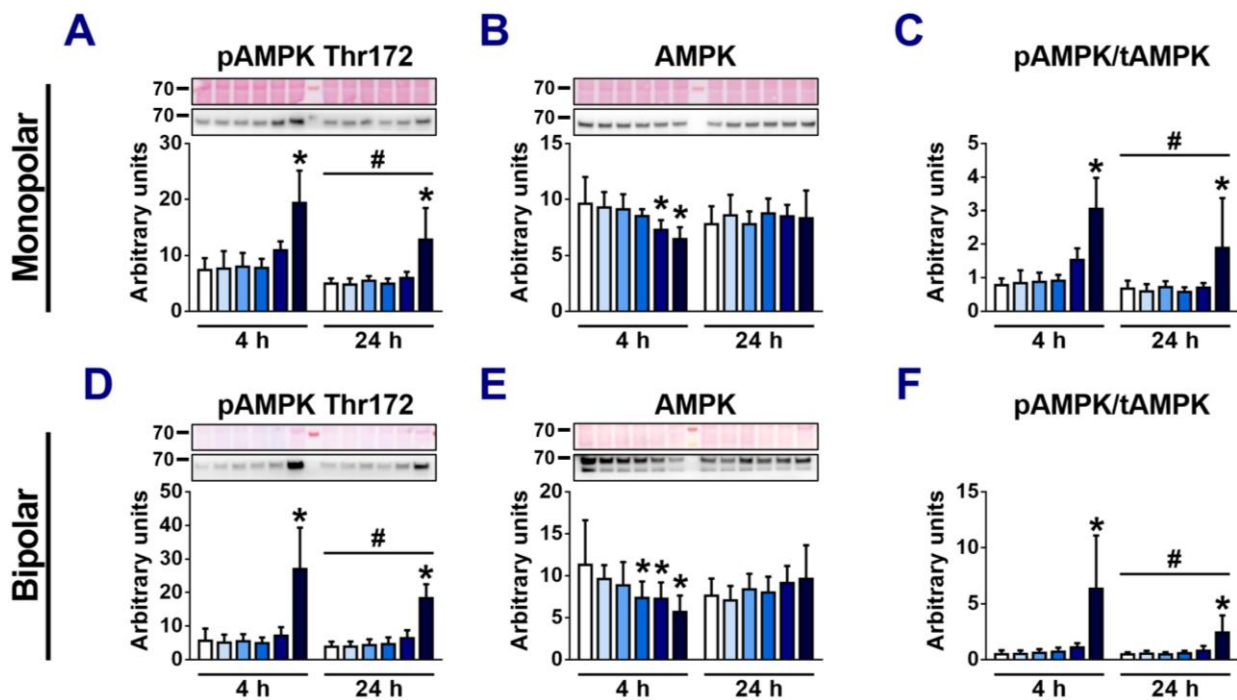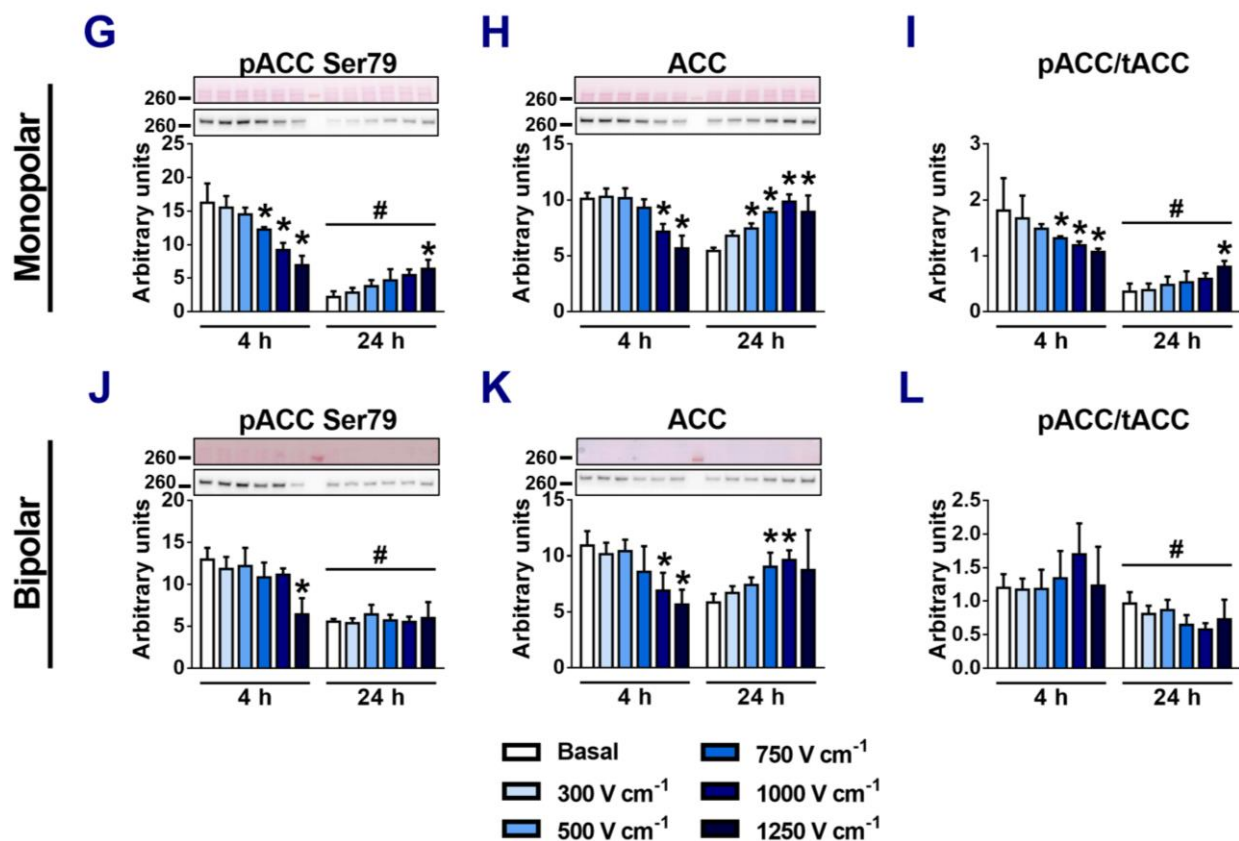

Figure 8. *Cont.*

Figure 8. Effects of electroporation with monopolar and bipolar pulses on phosphorylation and protein expression of AMPK and ACC in H9c2 cells. (**A–L**) Immunoblotting was used to estimate pAMPK Thr172, AMPK, phosphorylation of AMPK relative to total protein, pACC Ser79, ACC, and phosphorylation of ACC relative to total protein. Total protein loading was evaluated by Ponceau S staining (shown above the blots). Numbers next to the blots and Ponceau stains indicate molecular weight markers in kDa. Values on the graphs are means $\pm$ SD of at least three independent experiments (n = 4–8) and results that are statistically significant are indicated (*, $p < 0.05$; # $p < 0.05$ 4 h vs. 24 h; two-way ANOVA with Dunnet's post hoc adjustment).

The highest electric field tested (1250 V/cm) caused an increase in the phosphorylation of AMPK with both monopolar (Figure 8A) and H-FIRE pulses (Figure 8D); this was also true when the phosphorylated form was normalized to total protein (Figure 8C,F). ACC phosphorylation was decreased at 4 h with both monopolar and bipolar pulses (Figure 8G,J), but we observed an upregulation with monopolar pulses at 24 h (Figure 8G). The described trends were also significant for monopolar pulses when the phosphorylated form was normalized to total protein but not for bipolar pulses (Figure 8I,L).

4. Discussion

In this study, we show that the electroporation of H9c2 cells using two different waveforms, i.e., monopolar and H-FIRE pulses, at electric fields where a high percentage of permeabilization and low cell viability caused a dose-dependent downregulation in the expression of the most crucial isoforms of ion pump machinery. However, the only highly expressed subunits that were upregulated in electroporated samples were NKAα2 24 h after electroporation with both monopolar and H-FIRE pulses (Figure 5H,K) and NKAβ3 in cells treated with H-FIRE pulses (Figure 6L).

There are several isoforms of SERCA proteins expressed in mammalian tissues. They are coded by three genes, encoding for SERCA1, SERCA2, and SERCA3. Further variability is generated by alternative splicing [50]. In the mammalian heart, SERCA2a largely predominates, while SERCA2b represents a minor share [51]. SERCA2a activity is regulated

by two proteins, phospholamban (Pln) and sarcolipin (SLN). Both Pln and SLN inhibit the activity of SERCA2a, but it is known that the phosphorylation of Pln at two distinct sites disrupts the physical interaction of Pln with SERCA2a, which increases SERCA2a's activity [52]. Previous studies hypothesized that low SERCA and PMCA expression levels in some kinds of tumor cells may play a role in their high susceptibility to treatment with calcium electroporation, as their ability to excrete Ca^{2+} out of the cells or transport it into their ER/SR is limited. To our knowledge, no study has been published on how electroporation may affect the expression and activity of SERCA in cells after electroporation. Our results show that electroporation with both monopolar and H-FIRE pulses decreased the expression of SERCA1 and SERCA2. SERCA1 was decreased both at the mRNA and protein levels (Figure 4A,D,G,J), while SERCA2 downregulation was only observed at the protein level (Figure 4H,K). The presence of the SERCA1 isoform might be explained by the embryonic origin of H9c2 cells and their ability to differentiate into a skeletal muscle phenotype, as SERCA1 is normally not present in cardiac tissue, especially in adult ones [50]. We also investigated the expression of phospholamban. Unfortunately, we were only able to evaluate phospholamban at the mRNA level as we were unable to detect any bands at the protein level; thus, we could not determine how SERCA activity may be regulated through changes in the phosphorylation of phospholamban. Nevertheless, the exposure of cells to high electric fields with both monopolar and H-FIRE pulses decreased the expression of phospholamban 24 h after treatment (Figure 4I,L). Interestingly, phospholamban was significantly upregulated after 24 h compared to 4 h when looking at cells that underwent no treatment (basal), but exposure to high electric fields decreased mRNA expression to the basal levels of cells that were incubated for 4 h (Figure 4I,L). Due to surprising differences in basal mRNA levels between 4 and 24 h incubated cells, we tested whether the confluence of cells may play a role in the mRNA expression levels of phospholamban, as only a fraction of cells that are treated with high electric fields survive, which leads to lower confluency of seeded cells. We seeded cells at different dilutions with 4 and 24 h incubations and found that 24 h incubation significantly increased the mRNA expression of phospholamban compared to 4 h incubation when cells were seeded at high concentrations, but when the cell concentration was lowered, the mRNA expression levels dropped to the levels of cells incubated for 4 h (Supplementary Figure S1).

NKA is a heterodimer that consists of a catalytic α-subunit and a glycoprotein β-subunit. In the heart, α1, α2, α3, and β1 are expressed, while small amounts of β2 have also been detected [53]. In H9c2 cells, NKAα1 predominates (Figure 2), just like in mature rat and human cardiac tissue [54]. It was shown before that electroporation can affect the function of NKA in erythrocytes [33] and recently also that the silencing of genes for NKAα1 (ATP1A1) can attenuate the effects of nanopulses on membrane disruption in U937 human monocytes [55], but as with SERCAs, there are no studies that exploring how electroporation with different pulse protocols would affect the expression and activity of NKA. Our results show that treatment with high electric fields caused a downregulation in the protein content of NKAα1 24 and 4 h after treatment with monopolar (Figure 5G) and H-FIRE pulses (Figure 5J), respectively. On the other hand, we observed an upregulation in the protein content of NKAα2 24 h after treatment with both explored pulse parameters (Figure 5H,K). It is known that NKAα1 is nearly maximally activated at physiological ion levels [56,57], while NKAα2 is much more active when the membrane is depolarized and is a more important regulator of cardiac contractility, even though it is far less abundant than NKAα1. This may be of importance, as electroporated cells are in an extremely depolarized state due to nonselective membrane permeability allowing for the transport of ions through the plasma membrane [25,58,59].

NKA β-subunits are essential for the assembly, maturation, and function of α/β-heterodimers [60]. While we did see an upregulation in NKAβ1 at the mRNA level 4 h after electroporation (Figure 6A,D), this trend was not seen at the protein level. On the other hand, NKAβ3, which is also highly expressed in H9c2 cells due to their embryonic origin, was downregulated at the protein level 4 h after electroporation with both pulse

parameters (Figure 6I,L), but was upregulated 24 h after electroporation in cells exposed to H-FIRE pulses (Figure 6L). Due to the NKAβ subunit's importance in regulating the assembly of NKA heterodimers, its upregulation might play a role in more heterodimers reaching the cellular membrane, which could increase the cell's pumping capacity.

NKAs are regulated by proteins of the FXYD family, of which phospholemman (FXYD1) regulates NKA in heart and skeletal muscles [61,62]. While unphosphorylated FXYD1 inhibits NKA activity, its phosphorylated form increases NKA activity [62]. When we normalized the phosphorylated form of FXYD1 to total FXYD1 protein content, our results demonstrated that 24 h after electroporation, monopolar pulses may cause an inhibition in NKA activity (Figure 7I), while H-FIRE pulses only show a non-significant negative trend in the phosphorylation of FXYD1 (Figure 7L).

NKA activity is also regulated by the phosphorylation and glutathionylation of NKA itself, which affects its activity and its translocation to and from the sarcolemma [63]. We investigated the phosphorylation rates of NKAα1 on Tyrosine 10 residue, an under-researched phosphorylation site that may play an important role in the hormonal regulation of NKA. Here, we obtained divergent effects between two explored pulse parameters. Monopolar pulses did not seem to affect the phosphorylation of NKAα1 on Tyr10 (Figure 7A,B), while H-FIRE pulses increased it, even when normalized to total NKAα1 (Figure 7D,E).

Finally, we investigated potential AMPK activation by electroporation, an energy sensor that is activated in response to energy stress. It was shown by others that electroporation can lead to increased AMPK activity [41,49]. It is also known that AMPK can affect NKA and SERCA activity. We show that treatment with both monopolar and H-FIRE pulses at the highest electric fields caused the activation of AMPK in H9c2 cells, both 4 and 24 h after treatment (Figure 8A,C,D,F). Whether AMPK activation leads to increased or decreased NKA activity depends largely on the signaling pathway that causes AMPK activation. AMPK activation via the calcium/calmodulin-dependent protein kinase (CaMKK) signaling pathway decreased NKA activity in alveolar epithelial cells [64], while the activation of AMPK with AICAR, an AMP analogue in the rat L6 skeletal muscle cell line, increased NKA activity [39]. A769662, a direct activator of AMPK, also led to increased SERCA activity in freshly isolated vascular smooth muscle cells [40]. It was shown in human Jurkat cells and HeLa S3 cells that nanosecond pulses increase AMPK activity and that this increase can also be achieved via CaMKK [41]. Increased AMPK phosphorylation by CaMKK is achieved when Ca^{2+} levels in the cytosol are increased. This is also the case when cells are treated with monopolar and H-FIRE pulses, which may explain why the AMPK activation observed at high electric fields in our experiments correlates mostly with a decreased expression of NKA subunits in our experiments.

In the Introduction, we hypothesized that treatment with lower electric fields than lethal may lead to increased expression and activity of ion pumps, while higher electric fields where the majority of cells do not survive would cause a downregulation in expression and activity. Our hypothesis was based on prior studies, which showed that reversible electroporation leads to increased NKA activity in skeletal muscles [65,66]. We observed no increased expression of ion pumps at lower electric fields than lethal, and we observed no changes in the expression or activation of SERCA and NKA regulators, which may increase the activity of NKA or SERCA proteins.

In previous publications, our group showed that the effects of electroporation on cells can last for several hours or even days [32,46] and cause different types of cell death [16]. In the clinical use of electroporation (which includes PFA), both irreversible and reversible electroporation are present, as cells are exposed to different electroporation intensities, depending on their distance from the electrodes/catheter [67]. In this study, we were especially interested in what happens in cells that are reversibly electroporated and survive. Our protocol was, thus, designed in a way that we only evaluated mRNA and protein expression in cells that were still alive 4 or 24 h after electroporation. Nevertheless, it is possible that the population of cells, alive 4 and 24 h after electroporation, is not the same, which is also evident in some of our results, where the effects of electroporation with both

monopolar and H-FIRE pulses are different between cells that were incubated for 4 or 24 h. Overall, no major differences were observed between the effects of monopolar and H-FIRE pulses on the expression of the explored proteins. In the future, it may also be interesting to see how the expression of ion pumps is affected after a shorter incubation.

We need to acknowledge some limitations of this study. Firstly, we decided to use the H9c2 rat cardiac myoblast cell line, which has an embryonic origin and is derived from the left ventricle. While the ventricular origin of H9c2 cells can be considered a limitation of our study, we also state in the Introduction that there is a growing interest in using PFA in the treatment of ventricular arrhythmias, which makes the results of our study important for a deeper understanding of that application as well. It is important to note that even atrial cell lines, such as mouse HL-1 cells, differ quite significantly from primary cardiomyocytes. It was shown that, for example, regarding energy metabolic patterns, H9c2 cells are more like primary cardiomyocytes than HL-1 cells [68]. We, thus, propose that further studies should be performed on primary cardiomyocytes or induced pluripotent stem cell-derived cardiomyocytes, which are phenotypically more like cardiomyocytes, found in mature heart tissue. Secondly, it is important to note that we do not use exactly the same waveforms as commercially available for the PFA treatment of atrial fibrillation. However, since these waveforms are not disclosed by manufacturers, we performed experiments with two different types of pulses: monopolar relatively long 100 µs and H-FIRE-type pulses, i.e., short bipolar pulses, which we believe are representative of contemporary pulses. The results obtained using these different types of pulses were similar.

5. Conclusions

Our results indicate that the exposure of H9c2 cells to monopolar and H-FIRE pulses leads to a downregulation in the expression of most ion pump machinery proteins at the highest electric fields. It seems that decreased phosphorylation of FXYD1 at higher electric fields may inhibit NKA activity, and AMPK activation may be one of the mechanisms that downregulate both NKA and SERCA expression. Although we expected to see upregulation in the ion pumps at lower electric fields, we saw no evidence of that. Our results provide important new insights into what happens in surviving (and dying) cardiomyocytes after they are exposed to PFA. It will be important to further elucidate the possible signaling pathways that are involved in ion pump regulation in cells exposed to electroporation. This should also be performed on primary cardiomyocytes or induced pluripotent stem cell-derived cardiomyocytes, which are phenotypically more similar to cardiomyocytes found in mature heart tissue.

References

1. Padfield, G.J.; Steinberg, C.; Swampillai, J.; Qian, H.; Connolly, S.J.; Dorian, P.; Green, M.S.; Humphries, K.H.; Klein, G.J.; Sheldon, R.; et al. Progression of Paroxysmal to Persistent Atrial Fibrillation: 10-Year Follow-up in the Canadian Registry of Atrial Fibrillation. *Heart Rhythm* **2017**, *14*, 801–807. [CrossRef]

2. Hindricks, G.; Potpara, T.; Dagres, N.; Arbelo, E.; Bax, J.J.; Blomström-Lundqvist, C.; Boriani, G.; Castella, M.; Dan, G.-A.; Dilaveris, P.E.; et al. 2020 ESC Guidelines for the Diagnosis and Management of Atrial Fibrillation Developed in Collaboration with the European Association for Cardio-Thoracic Surgery (EACTS). *Eur. Heart J.* **2021**, *42*, 373–498. [CrossRef]

3. Verma, A.; Asivatham, S.J.; Deneke, T.; Castellvi, Q.; Neal, R.E. Primer on Pulsed Electrical Field Ablation: Understanding the Benefits and Limitations. *Circ. Arrhythmia Electrophysiol.* **2021**, *14*, e010086. [CrossRef] [PubMed]

4. Bradley, C.J.; Haines, D.E. Pulsed Field Ablation for Pulmonary Vein Isolation in the Treatment of Atrial Fibrillation. *Cardiovasc. Electrophysiol.* **2020**, *31*, 2136–2147. [CrossRef] [PubMed]

5. Reddy, V.Y.; Neuzil, P.; Koruth, J.S.; Petru, J.; Funosako, M.; Cochet, H.; Sediva, L.; Chovanec, M.; Dukkipati, S.R.; Jais, P. Pulsed Field Ablation for Pulmonary Vein Isolation in Atrial Fibrillation. *J. Am. Coll. Cardiol.* **2019**, *74*, 315–326. [CrossRef] [PubMed]

6. Reddy, V.Y.; Koruth, J.; Jais, P.; Petru, J.; Timko, F.; Skalsky, I.; Hebeler, R.; Labrousse, L.; Barandon, L.; Kralovec, S.; et al. Ablation of Atrial Fibrillation With Pulsed Electric Fields. *JACC Clin. Electrophysiol.* **2018**, *4*, 987–995. [CrossRef] [PubMed]

7. Nakagawa, H.; Castellvi, Q.; Neal, R.; Girouard, S.; Laughner, J.; Ikeda, A.; Sugawara, M.; An, Y.; Hussein, A.A.; Nakhla, S.; et al. Effects of Contact Force on Lesion Size During Pulsed Field Catheter Ablation: Histochemical Characterization of Ventricular Lesion Boundaries. *Circ. Arrhythmia Electrophysiol.* **2024**, *17*, e012026. [CrossRef]

8. Tan, N.Y.; Ladas, T.P.; Christopoulos, G.; Sugrue, A.M.; Van Zyl, M.; Ladejobi, A.O.; Lodhi, F.K.; Hu, T.Y.; Ezzeddine, F.M.; Agboola, K.; et al. Ventricular Nanosecond Pulsed Electric Field Delivery Using Active Fixation Leads: A Proof-of-Concept Preclinical Study. *J. Interv. Card. Electrophysiol.* **2022**. [CrossRef] [PubMed]

9. Sandhu, U.; Alkukhun, L.; Kheiri, B.; Hodovan, J.; Chiang, K.; Splanger, T.; Castellvi, Q.; Zhao, Y.; Nazer, B. In Vivo Pulsed-Field Ablation in Healthy vs. Chronically Infarcted Ventricular Myocardium: Biophysical and Histologic Characterization. *EP Eur.* **2023**, *25*, 1503–1509. [CrossRef]

10. Ouss, A.; Van Stratum, L.; Van Der Voort, P.; Dekker, L. First in Human Pulsed Field Ablation to Treat Scar-Related Ventricular Tachycardia in Ischemic Heart Disease: A Case Report. *J. Interv. Card. Electrophysiol.* **2022**, *66*, 509–510. [CrossRef]

11. Younis, A.; Zilberman, I.; Krywanczyk, A.; Higuchi, K.; Yavin, H.D.; Sroubek, J.; Anter, E. Effect of Pulsed-Field and Radiofrequency Ablation on Heterogeneous Ventricular Scar in a Swine Model of Healed Myocardial Infarction. *Circ. Arrhythmia Electrophysiol.* **2022**, *15*, e011209. [CrossRef]

12. Im, S.I.; Higuchi, S.; Lee, A.; Stillson, C.; Buck, E.; Morrow, B.; Schenider, K.; Speltz, M.; Gerstenfeld, E.P. Pulsed Field Ablation of Left Ventricular Myocardium in a Swine Infarct Model. *JACC Clin. Electrophysiol.* **2022**, *8*, 722–731. [CrossRef]

13. Sugrue, A.; Vaidya, V.R.; Livia, C.; Padmanabhan, D.; Abudan, A.; Isath, A.; Witt, T.; DeSimone, C.V.; Stalboerger, P.; Kapa, S.; et al. Feasibility of Selective Cardiac Ventricular Electroporation. *PLoS ONE* **2020**, *15*, e0229214. [CrossRef] [PubMed]

14. Kotnik, T.; Rems, L.; Tarek, M.; Miklavčič, D. Membrane Electroporation and Electropermeabilization: Mechanisms and Models. *Annu. Rev. Biophys.* **2019**, *48*, 63–91. [CrossRef] [PubMed]

15. Hartl, S.; Reinsch, N.; Füting, A.; Neven, K. Pearls and Pitfalls of Pulsed Field Ablation. *Korean Circ. J.* **2023**, *53*, 273. [CrossRef] [PubMed]

16. Batista Napotnik, T.; Polajžer, T.; Miklavčič, D. Cell Death Due to Electroporation—A Review. *Bioelectrochemistry* **2021**, *141*, 107871. [CrossRef] [PubMed]

17. Reddy, V.Y.; Gerstenfeld, E.P.; Natale, A.; Whang, W.; Cuoco, F.A.; Patel, C.; Mountantonakis, S.E.; Gibson, D.N.; Harding, J.D.; Ellis, C.R.; et al. Pulsed Field or Conventional Thermal Ablation for Paroxysmal Atrial Fibrillation. *N. Engl. J. Med.* **2023**, *389*, 1660–1671. [CrossRef]

18. Verma, A.; Haines, D.E.; Boersma, L.V.; Sood, N.; Natale, A.; Marchlinski, F.E.; Calkins, H.; Sanders, P.; Packer, D.L.; Kuck, K.-H.; et al. Pulsed Field Ablation for the Treatment of Atrial Fibrillation: PULSED AF Pivotal Trial. *Circulation* **2023**, *147*, 1422–1432. [CrossRef]

19. Howard, B.; Haines, D.E.; Verma, A.; Packer, D.; Kirchhof, N.; Barka, N.; Onal, B.; Fraasch, S.; Miklavčič, D.; Stewart, M.T. Reduction in Pulmonary Vein Stenosis and Collateral Damage With Pulsed Field Ablation Compared With Radiofrequency Ablation in a Canine Model. *Circ. Arrhythmia Electrophysiol.* **2020**, *13*, e008337. [CrossRef]

20. Stewart, M.T.; Haines, D.E.; Miklavčič, D.; Kos, B.; Kirchhof, N.; Barka, N.; Mattison, L.; Martien, M.; Onal, B.; Howard, B.; et al. Safety and Chronic Lesion Characterization of Pulsed Field Ablation in a Porcine Model. *J. Cardiovasc. Electrophysiol.* **2021**, *32*, 958–969. [CrossRef]

21. Cvetkoska, A.; Maček-Lebar, A.; Polajžer, T.; Reberšek, M.; Upchurch, W.; Iaizzo, P.A.; Sigg, D.C.; Miklavčič, D. The Effects of Interphase and Interpulse Delays and Pulse Widths on Induced Muscle Contractions, Pain and Therapeutic Efficacy in Electroporation-Based Therapies. *JCDD* **2023**, *10*, 490. [CrossRef]

22. Koruth, J.S.; Neuzil, P.; Kawamura, I.; Kuroki, K.; Petru, J.; Rackauskas, G.; Funasako, M.; Aidietis, A.; Reddy, V.Y. Reversible Pulsed Electrical Fields as an In Vivo Tool to Study Cardiac Electrophysiology: The Advent of Pulsed Field Mapping. *Circ. Arrhythmia Electrophysiol.* **2023**, *16*, e012018. [CrossRef]

23. Chaigne, S.; Sigg, D.C.; Stewart, M.T.; Hocini, M.; Batista Napotnik, T.; Miklavčič, D.; Bernus, O.; Benoist, D. Reversible and Irreversible Effects of Electroporation on Contractility and Calcium Homeostasis in Isolated Cardiac Ventricular Myocytes. *Circ. Arrhythm Electrophysiol.* **2022**, *15*, e011131. [CrossRef] [PubMed]

24. Hunter, D.W.; Kostecki, G.; Fish, J.M.; Jensen, J.A.; Tandri, H. In Vitro Cell Selectivity of Reversible and Irreversible: Electroporation in Cardiac Tissue. *Circ. Arrhythmia Electrophysiol.* **2021**, *14*, e008817. [CrossRef] [PubMed]

25. Tung, L.; Tovar, O.; Neunlist, M.; Jain, S.K.; O'Neill, R.J. Effects of Strong Electrical Shock on Cardiac Muscle Tissuea. *Ann. N. Y. Acad. Sci.* **1994**, *720*, 160–175. [CrossRef] [PubMed]

26. Rems, L.; Kasimova, M.A.; Testa, I.; Delemotte, L. Pulsed Electric Fields Can Create Pores in the Voltage Sensors of Voltage-Gated Ion Channels. *Biophys. J.* **2020**, *119*, 190–205. [CrossRef]

27. Doenst, T.; Nguyen, T.D.; Abel, E.D. Cardiac Metabolism in Heart Failure: Implications Beyond ATP Production. *Circ. Res.* **2013**, *113*, 709–724. [CrossRef] [PubMed]

28. Gibbs, C.L. Cardiac Energetics. *Physiol. Rev.* **1978**, *58*, 174–254. [CrossRef]

29. Suga, H. Ventricular Energetics. *Physiol. Rev.* **1990**, *70*, 247–277. [CrossRef]

30. Frandsen, S.K.; Vissing, M.; Gehl, J. A Comprehensive Review of Calcium Electroporation—A Novel Cancer Treatment Modality. *Cancers* **2020**, *12*, 290. [CrossRef]

31. Frandsen, S.K.; Gissel, H.; Hojman, P.; Tramm, T.; Eriksen, J.; Gehl, J. Direct Therapeutic Applications of Calcium Electroporation to Effectively Induce Tumor Necrosis. *Cancer Res.* **2012**, *72*, 1336–1341. [CrossRef]

32. Polajžer, T.; Miklavčič, D. Immunogenic Cell Death in Electroporation-Based Therapies Depends on Pulse Waveform Characteristics. *Vaccines* **2023**, *11*, 1036. [CrossRef]

33. Teissie, J.; Tsong, T.Y. Evidence of Voltage-Induced Channel Opening in Na/K ATPase of Human Erythrocyte Membrane. *J. Membrain Biol.* **1980**, *55*, 133–140. [CrossRef]

34. Hardie, D.G.; Hawley, S.A. AMP-Activated Protein Kinase: The Energy Charge Hypothesis Revisited. *Bioessays* **2001**, *23*, 1112–1119. [CrossRef]

35. Hardie, D.G. Molecular Pathways: Is AMPK a Friend or a Foe in Cancer? *Clin. Cancer Res.* **2015**, *21*, 3836–3840. [CrossRef] [PubMed]

36. Hardie, D.G.; Ross, F.A.; Hawley, S.A. AMPK: A Nutrient and Energy Sensor That Maintains Energy Homeostasis. *Nat. Rev. Mol. Cell Biol.* **2012**, *13*, 251–262. [CrossRef]

37. Ono, H.; Suzuki, N.; Kanno, S.; Kawahara, G.; Izumi, R.; Takahashi, T.; Kitajima, Y.; Osana, S.; Nakamura, N.; Akiyama, T.; et al. AMPK Complex Activation Promotes Sarcolemmal Repair in Dysferlinopathy. *Mol. Ther.* **2020**, *28*, 1133–1153. [CrossRef] [PubMed]

38. Grahame Hardie, D. Regulation of AMP-Activated Protein Kinase by Natural and Synthetic Activators. *Acta Pharm. Sin. B* **2016**, *6*, 1–19. [CrossRef]

39. Benziane, B.; Björnholm, M.; Pirkmajer, S.; Austin, R.L.; Kotova, O.; Viollet, B.; Zierath, J.R.; Chibalin, A.V. Activation of AMP-Activated Protein Kinase Stimulates Na$^+$,K$^+$-ATPase Activity in Skeletal Muscle Cells. *J. Biol. Chem.* **2012**, *287*, 23451–23463. [CrossRef]

40. Schneider, H.; Schubert, K.M.; Blodow, S.; Kreutz, C.-P.; Erdogmus, S.; Wiedenmann, M.; Qiu, J.; Fey, T.; Ruth, P.; Lubomirov, L.T.; et al. AMPK Dilates Resistance Arteries via Activation of SERCA and BK$_{Ca}$ Channels in Smooth Muscle. *Hypertension* **2015**, *66*, 108–116. [CrossRef] [PubMed]

41. Morotomi-Yano, K.; Akiyama, H.; Yano, K. Nanosecond Pulsed Electric Fields Activate AMP-Activated Protein Kinase: Implications for Calcium-Mediated Activation of Cellular Signaling. *Biochem. Biophys. Res. Commun.* **2012**, *428*, 371–375. [CrossRef]

42. Dermol-Černe, J.; Miklavčič, D.; Reberšek, M.; Mekuč, P.; Bardet, S.M.; Burke, R.; Arnaud-Cormos, D.; Leveque, P.; O'Connor, R. Plasma Membrane Depolarization and Permeabilization Due to Electric Pulses in Cell Lines of Different Excitability. *Bioelectrochemistry* **2018**, *122*, 103–114. [CrossRef]

43. Raso, J.; Frey, W.; Ferrari, G.; Pataro, G.; Knorr, D.; Teissie, J.; Miklavčič, D. Recommendations Guidelines on the Key Information to Be Reported in Studies of Application of PEF Technology in Food and Biotechnological Processes. *Innov. Food Sci. Emerg. Technol.* **2016**, *37*, 312–321. [CrossRef]

44. Cemazar, M.; Sersa, G.; Frey, W.; Miklavcic, D.; Teissié, J. Recommendations and Requirements for Reporting on Applications of Electric Pulse Delivery for Electroporation of Biological Samples. *Bioelectrochemistry* **2018**, *122*, 69–76. [CrossRef] [PubMed]

45. Campana, L.G.; Clover, A.J.P.; Valpione, S.; Quaglino, P.; Gehl, J.; Kunte, C.; Snoj, M.; Cemazar, M.; Rossi, C.R.; Miklavcic, D.; et al. Recommendations for Improving the Quality of Reporting Clinical Electrochemotherapy Studies Based on Qualitative Systematic Review. *Radiol. Oncol.* **2016**, *50*, 1–13. [CrossRef] [PubMed]

46. Peng, W.; Polajžer, T.; Yao, C.; Miklavčič, D. Dynamics of Cell Death Due to Electroporation Using Different Pulse Parameters as Revealed by Different Viability Assays. *Ann. Biomed. Eng.* **2023**, *52*, 22–35. [CrossRef] [PubMed]

47. Ruijter, J.M.; Ramakers, C.; Hoogaars, W.M.H.; Karlen, Y.; Bakker, O.; Van Den Hoff, M.J.B.; Moorman, A.F.M. Amplification Efficiency: Linking Baseline and Bias in the Analysis of Quantitative PCR Data. *Nucleic Acids Res.* **2009**, *37*, e45. [CrossRef] [PubMed]

48. Tuomi, J.M.; Voorbraak, F.; Jones, D.L.; Ruijter, J.M. Bias in the Cq Value Observed with Hydrolysis Probe Based Quantitative PCR Can Be Corrected with the Estimated PCR Efficiency Value. *Methods* **2010**, *50*, 313–322. [CrossRef] [PubMed]

49. Frandsen, S.K.; Gehl, J. Effect of Calcium Electroporation in Combination with Metformin in Vivo and Correlation between Viability and Intracellular ATP Level after Calcium Electroporation in Vitro. *PLoS ONE* **2017**, *12*, e0181839. [CrossRef] [PubMed]

50. Periasamy, M.; Kalyanasundaram, A. SERCA Pump Isoforms: Their Role in Calcium Transport and Disease. *Muscle Nerve* **2007**, *35*, 430–442. [CrossRef]

51. Dally, S.; Corvazier, E.; Bredoux, R.; Bobe, R.; Enouf, J. Multiple and Diverse Coexpression, Location, and Regulation of Additional SERCA2 and SERCA3 Isoforms in Nonfailing and Failing Human Heart. *J. Mol. Cell. Cardiol.* **2010**, *48*, 633–644. [CrossRef]

52. Bhupathy, P.; Babu, G.J.; Ito, M.; Periasamy, M. Threonine-5 at the N-Terminus Can Modulate Sarcolipin Function in Cardiac Myocytes. *J. Mol. Cell. Cardiol.* **2009**, *47*, 723–729. [CrossRef]

53. McDonough, A.A.; Velotta, J.B.; Schwinger, R.H.G.; Philipson, K.D.; Farley, R.A. The Cardiac Sodium Pump: Structure and Function. *Basic Res. Cardiol.* **2002**, *97*, I19–I24. [CrossRef]

54. Skogestad, J.; Aronsen, J.M. Regulation of Cardiac Contractility by the Alpha 2 Subunit of the Na^+/K^+-ATPase. *Front. Physiol.* **2022**, *13*, 827334. [CrossRef] [PubMed]

55. Silkuniene, G.; Mangalanathan, U.M.; Pakhomov, A.G.; Pakhomova, O.N. Silencing of ATP1A1 Attenuates Cell Membrane Disruption by Nanosecond Electric Pulses. *Biochem. Biophys. Res. Commun.* **2023**, *677*, 93–97. [CrossRef] [PubMed]

56. Han, F.; Tucker, A.L.; Lingrel, J.B.; Despa, S.; Bers, D.M. Extracellular Potassium Dependence of the Na^+-K^+-ATPase in Cardiac Myocytes: Isoform Specificity and Effect of Phospholemman. *Am. J. Physiol.-Cell Physiol.* **2009**, *297*, C699–C705. [CrossRef]

57. Stanley, C.M.; Gagnon, D.G.; Bernal, A.; Meyer, D.J.; Rosenthal, J.J.; Artigas, P. Importance of the Voltage Dependence of Cardiac Na/K ATPase Isozymes. *Biophys. J.* **2015**, *109*, 1852–1862. [CrossRef]

58. Pakhomov, A.G.; Kolb, J.F.; White, J.A.; Joshi, R.P.; Xiao, S.; Schoenbach, K.H. Long-lasting Plasma Membrane Permeabilization in Mammalian Cells by Nanosecond Pulsed Electric Field (nsPEF). *Bioelectromagnetics* **2007**, *28*, 655–663. [CrossRef] [PubMed]

59. Batista Napotnik, T.; Kos, B.; Jarm, T.; Miklavčič, D.; O'Connor, R.P.; Rems, L. Genetically Engineered HEK Cells as a Valuable Tool for Studying Electroporation in Excitable Cells. *Sci. Rep.* **2024**, *14*, 720. [CrossRef] [PubMed]

60. Ackermann, U.; Geering, K. Mutual Dependence of Na,K-ATPase A- and B-subunits for Correct Posttranslational Processing and Intracellular Transport. *FEBS Lett.* **1990**, *269*, 105–108. [CrossRef]

61. Therien, A.G.; Blostein, R. Mechanisms of Sodium Pump Regulation. *Am. J. Physiol.-Cell Physiol.* **2000**, *279*, C541–C566. [CrossRef] [PubMed]

62. Crambert, G.; Füzesi, M.; Garty, H.; Karlish, S.; Geering, K. Phospholemman (FXYD1) Associates with Na,K-ATPase and Regulates Its Transport Properties. *Proc. Natl. Acad. Sci. USA* **2002**, *99*, 11476–11481. [CrossRef] [PubMed]

63. Pirkmajer, S.; Chibalin, A.V. Na,K-ATPase Regulation in Skeletal Muscle. *Am. J. Physiol.-Endocrinol. Metab.* **2016**, *311*, E1–E31. [CrossRef]

64. Gusarova, G.A.; Trejo, H.E.; Dada, L.A.; Briva, A.; Welch, L.C.; Hamanaka, R.B.; Mutlu, G.M.; Chandel, N.S.; Prakriya, M.; Sznajder, J.I. Hypoxia Leads to Na,K-ATPase Downregulation via Ca^{2+} Release-Activated Ca^{2+} Channels and AMPK Activation. *Mol. Cell. Biol.* **2011**, *31*, 3546–3556. [CrossRef] [PubMed]

65. Buchanan, R.; Nielsen, O.B.; Clausen, T. Excitation- and β_2-agonist-induced Activation of the Na^+−K^+ Pump in Rat Soleus Muscle. *J. Physiol.* **2002**, *545*, 229–240. [CrossRef]

66. Clausen, T.; Gissel, H. Role of Na^+, K^+ Pumps in Restoring Contractility Following Loss of Cell Membrane Integrity in Rat Skeletal Muscle. *Acta Physiol. Scand.* **2005**, *183*, 263–271. [CrossRef]

67. Cindrič, H.; Kos, B.; Miklavčič, D. Electrodes and Electric Field Distribution in Clinical Practice. In *Electroporation in Veterinary Oncology Practice*; Impellizeri, J.A., Ed.; Springer International Publishing: Cham, Switzerland, 2021; pp. 21–59. ISBN 978-3-030-80667-5.

68. Kuznetsov, A.V.; Javadov, S.; Sickinger, S.; Frotschnig, S.; Grimm, M. H9c2 and HL-1 Cells Demonstrate Distinct Features of Energy Metabolism, Mitochondrial Function and Sensitivity to Hypoxia-Reoxygenation. *Biochim. Et Biophys. Acta (BBA)-Mol. Cell Res.* **2015**, *1853*, 276–284. [CrossRef]